Cryptic oxygen cycling in anoxic marine zones.

Emilio Garcia-Robledo, Cory C Padilla, Montserrat Aldunate, Frank J
Stewart, Osvaldo Ulloa, Aurélien Paulmier, Gérald Grégori, Niels Peter
Revsbech

HAL Id: hal-01580084
https://hal.science/hal-01580084

Submitted on 19 Feb 2019

Cryptic oxygen cycling in anoxic marine zones

Emilio Garcia-Robledo[a,1,2], Cory C. Padilla[b], Montserrat Aldunate[c,d], Frank J. Stewart[b], Osvaldo Ulloa[d], Aurélien Paulmier[e], Gerald Gregori[f], and Niels Peter Revsbech[a]

[a]Microbiology Section, Department of Bioscience, Aarhus University, 8000 Aarhus, Denmark; [b]School of Biological Sciences, Georgia Institute of Technology, Atlanta, GA 30332-0230; [c]Graduate Program in Oceanography, Department of Oceanography, University of Concepción, 4070386 Concepcion, Chile; [d]Departamento de Oceanografía, Instituto Milenio de Oceanografía, Universidad de Concepción, 4070386 Concepción, Chile; [e]Laboratoire d'Etudes en Géophysique et Océanographie Spatiales, Institut de Recherche pour le Développement, CNRS, Centre National d'Etudes Spatiales, University of Toulouse, 31400 Toulouse, France; and [f]Aix Marseille Université, Université de Toulon, CNRS, Institut pour la Recherche et le Développement, Mediterranean Institute of Oceanography UM 110, 13288 Marseille, France

Oxygen availability drives changes in microbial diversity and biogeochemical cycling between the aerobic surface layer and the anaerobic core in nitrite-rich anoxic marine zones (AMZs), which constitute huge oxygen-depleted regions in the tropical oceans. The current paradigm is that primary production and nitrification within the oxic surface layer fuel anaerobic processes in the anoxic core of AMZs, where 30–50% of global marine nitrogen loss takes place. Here we demonstrate that oxygenic photosynthesis in the secondary chlorophyll maximum (SCM) releases significant amounts of O_2 to the otherwise anoxic environment. The SCM, commonly found within AMZs, was dominated by the picocyanobacteria *Prochlorococcus* spp. Free O_2 levels in this layer were, however, undetectable by conventional techniques, reflecting a tight coupling between O_2 production and consumption by aerobic processes under apparent anoxic conditions. Transcriptomic analysis of the microbial community in the seemingly anoxic SCM revealed the enhanced expression of genes for aerobic processes, such as nitrite oxidation. The rates of gross O_2 production and carbon fixation in the SCM were found to be similar to those reported for nitrite oxidation, as well as for anaerobic dissimilatory nitrate reduction and sulfate reduction, suggesting a significant effect of local oxygenic photosynthesis on Pacific AMZ biogeochemical cycling.

Prochlorococcus | oxygen minimum zone | secondary chlorophyll maximum | metatranscriptomics | aerobic metabolism

In coastal zones of the eastern tropical Pacific Ocean, the upward transportation of nutrient-rich waters results in relatively high primary productivity at surface depths. Sinking of organic matter produced by surface production coupled with sluggish circulation leads to the formation of oxygen-deficient water masses at intermediate depths below the mixed layer. Due to strong stratification, these oxygen minimum zones (OMZs) extend far offshore over vast swaths of the eastern Pacific. In these regions, oxygen availability plays a major role in structuring organism distributions and biogeochemical processes in the pelagic ocean (1).

Recently developed sensor techniques (2) show that in much of the OMZ water column, from about 30–100 m to about 800 m, O_2 concentrations fall below sensor-specific detection limits of down to 3 nmol·L^{-1} ($3·10^{-9}$ moles per liter) (3, 4). OMZs in the eastern tropical North and South Pacific (ETNP and ETSP, respectively) and in the Arabian Sea are subject to such intense O_2 depletion and therefore have been redefined as anoxic marine zones (AMZs) (5). In other oceanic OMZs, including in the Bay of Bengal and northeast Pacific, oxygen concentrations may decrease to a few micromolar, but total O_2 depletion occurs only occasionally (6). AMZs are often distinguished from more oxygen-replete OMZs by the accumulation of nitrite, which is typically most pronounced when O_2 falls below the nanomolar detection limit (5–8). Nitrite is a key substrate in microbial N_2 and N_2O production by either denitrification or anaerobic ammonium oxidation (anammox), which together in AMZs mediate 30–50% (9) of the marine recycling of inorganic nitrogen compounds (nitrate, nitrite, and ammonium) to atmospheric N_2.

Nitrite is also produced and consumed in the aerobic nitrification pathway involving the two-step process of aerobic ammonia and nitrite oxidation (10, 11). Despite the absence of measureable O_2 in the core of eastern Pacific AMZs, biomolecular evidence (DNA, RNA, and proteins) indicates the presence of aerobic microbial processes. The expression of genes encoding for nitrification and other O_2-dependent microbial metabolisms, potentially including heterotrophic respiration, have been found well below the oxycline (12, 13), raising the question of how aerobic processes could persist under apparent anoxia.

In the three oceanic AMZs of the Arabian Sea, ETNP, and ETSP, dense populations of phototrophs have been observed at the base of the photic zone but below the oxycline that separates oxic from anoxic waters (14–16). This deep secondary chlorophyll maximum (SCM) is mainly composed of novel, yet uncultivated, lineages of the cyanobacterium *Prochlorococcus* (14), with chlorophyll concentrations that can equal that of the primary chlorophyll peak near the surface (16). The presence of this large population of putative oxygenic phototrophs has suggested a mechanism by which aerobic metabolism can be maintained in a zone where in situ measurements indicate anoxic conditions (5). Although an active photosynthetic community produces and releases oxygen to the environment, coupled O_2 consumption by an aerobic microbial community may keep seawater O_2 concentration at very low and possibly subnanomolar levels, thereby resulting in a cryptic O_2 cycle. The existence of such a cryptic

Significance

Anoxic marine zones (AMZs) create expansive habitats for microbes whose anaerobic metabolisms help drive global nutrient cycles, for example, by removing nitrogen from the oceans by producing N_2 gas. AMZ cycles may also be shaped by oxygen intrusion from outside the AMZ, creating opportunities for aerobic microbial metabolisms. Here we show that aerobic processes in AMZs are linked to oxygen production within the anoxic zone. Oxygen is produced during daytime in a layer of photosynthetic cyanobacteria near the top of the AMZ and then rapidly consumed by aerobic processes without accumulating. Oxygen turnover and carbon fixation rates are comparable to those of microbial N_2 production, suggesting an important role for internal oxygen cycling in AMZ transformations of matter and energy.

oxygen cycle has been suggested by biomolecular evidence (12) but has not yet been demonstrated.

In this study we used a combination of high-resolution oxygen profiling, metabolic rate measurements, and community mRNA sequencing to explore the potential for oxygen cycling in the SCMs of the ETNP off Mexico and the ETSP off Peru. Our results show that the photosynthetic community of the SCM produces significant amounts of O_2, sufficient to maintain an aerobic community in an otherwise anoxic environment. Rates of O_2 production and carbon fixation in the SCM in both ETNP and ETSP AMZs are comparable to previously measured rates of aerobic processes like nitrite and ammonium oxidation (8, 17), as well as anaerobic AMZ processes like denitrification, anammox, and sulfate reduction (7, 8). Although the measured metabolic rates exhibit large spatial and temporal variability, our data collectively suggest a significant effect of local photosynthesis on the biogeochemical cycling in Pacific Ocean AMZs.

Results and Discussion

Sampling in both the ETNP and ETSP revealed a typical AMZ O_2 distribution in the upper 200 m of the water column. Oxygen concentrations in the 0–35 m surface layer in the ETNP were stable at ~200 $\mu mol \cdot kg^{-1}$, before declining along a clearly defined oxycline from 35–45 to 60–80 m, and then falling below the detection limit of the switchable trace amount oxygen (STOX) sensors (few nanometers) at 80–100 m (Fig. 1B). In the ETSP AMZ off Peru, O_2 concentrations and the depth of the oxycline were more variable and clearly influenced by proximity to the shore, with anoxic depths beginning at ~30 m at the coastal station but at ~70 m for the more oceanic station (Fig. 1H). In both the ETNP and ETSP, the chlorophyll concentration below

the primary maximum decreased in parallel with O_2 concentration, reaching a minimum before complete O_2 depletion and then increasing again to form an SCM in which 90% of the phototrophs were *Prochlorococcus* (Fig. 1 and Table S1). Although the upper region of the SCM was consistently located near the oxic–anoxic interface, maximum in vivo fluorescence and *Prochlorococcus* abundance were usually localized within the anoxic zone a few meters below. Low O_2 concentrations (<500 $nmol \cdot L^{-1}$) were occasionally found inside the SCM (Table S2), suggesting intrusion of overlying oxygenated waters or in situ O_2 production and accumulation.

Oxygenic Photosynthesis and Carbon Fixation in the SCM. Shipboard experiments using water from the SCM incubated under trace O_2 conditions revealed that O_2 concentration with time differed substantially between dark- and light-incubated samples (Fig. 2 A and D). Net community production (NCP), corresponding to the slope of the O_2 concentration curves and hence the balance between O_2 production and consumption, gradually increased to more positive values with increasing irradiance. NCP was also variable between stations, reflecting the spatial and temporal variability of the metabolic activity in terms of photosynthesis and respiration rates (Fig. 2 B and E). At several stations, net consumption of O_2 occurred at all applied irradiances, although a clear decrease in consumption rate was always measured with increasing light intensities. At other stations, a net increase in O_2 was measured when the samples were exposed to an irradiance of only 10 μmol photons$\cdot m^{-2} \cdot s^{-1}$. The observed maximum irradiance in situ was, however, only in the range of 2–5 μmol photons$\cdot m^{-2} \cdot s^{-1}$ at most stations (see examples in Fig. S1); at such low light levels, net O_2 consumption was always observed.
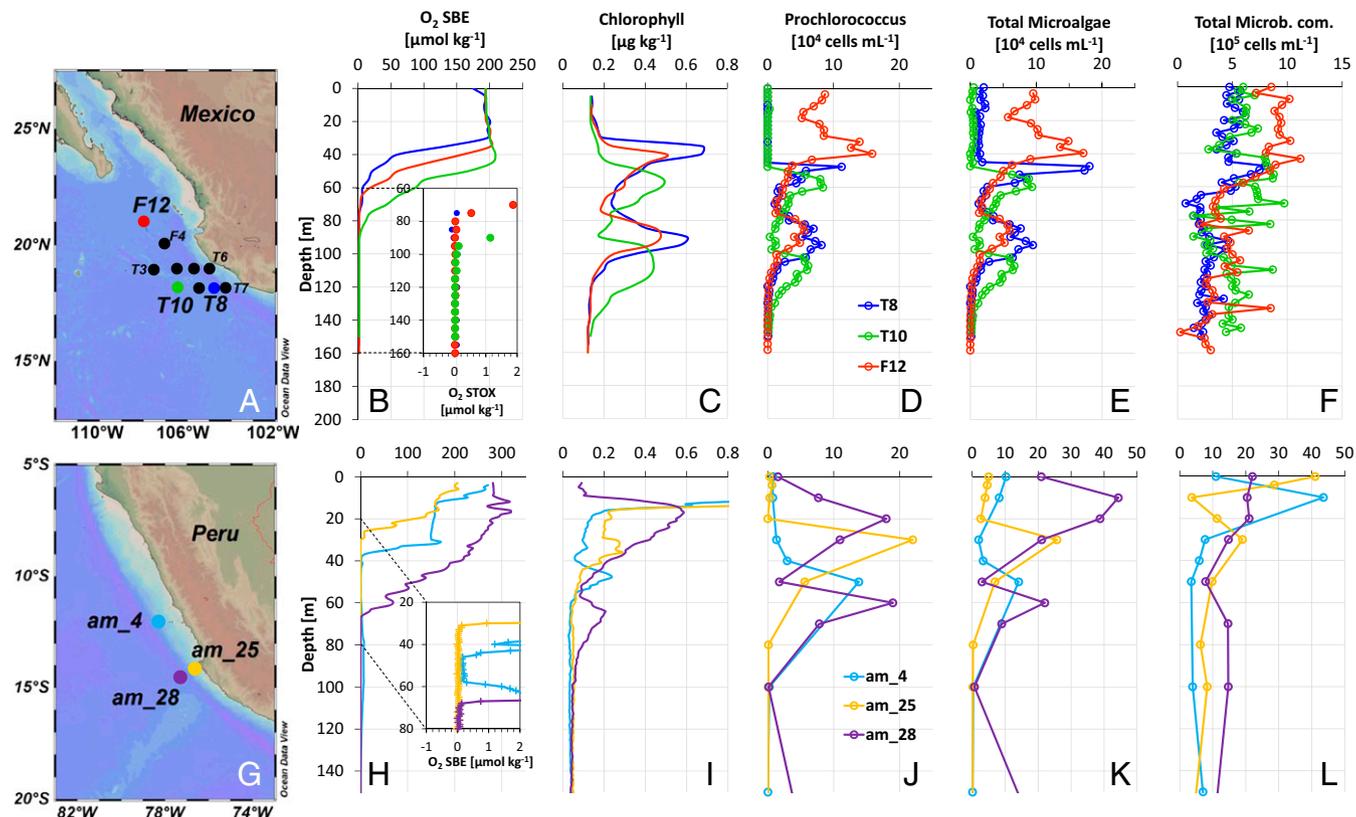
Fig. 1. Maps with sampled stations and main characteristics of the upper part of the (*A–F*) ETNP AMZ and (*G–L*) ETSP AMZ. Stations off Mexico (*A*) and Peru (*G*) where the SCM was found and sampled. (*B* and *H*) Dissolved oxygen profiles, based on SBE43 and STOX sensors (zooming in at low STOX O_2 values in *B* or corrected SBE O_2 in *H*). (*C* and *I*) Profiles of chlorophyll concentration inferred from in vivo fluorescence. (*D* and *J*) *Prochlorococcus* abundance. (*E* and *K*) Total microalgae (*Prochlorococcus*, *Synechococcus*, and picoeukaryotes) and (*F* and *L*) total microbial community (Total Microb. com.) abundance measured by flow cytometry.
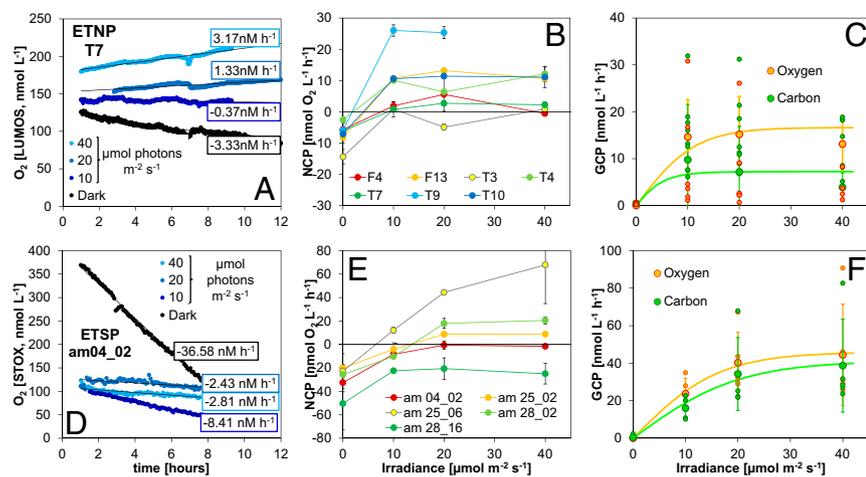
Fig. 2. Oxygen production and carbon fixation during incubations of samples from the SCM off (A–C) Mexico and (D–F) Peru. (A and D) Evolution of O_2 concentration during incubation of SCM samples exposed to a range of scalar irradiances (0–40 μmol photons·m^{-2}·s^{-1}). (B and E) Net community production (NCP) rates versus scalar irradiance. (C and F) Gross community production (GCP): O_2-GCP was measured as the net O_2 production, and C-GCP was measured by the incorporation of ^{13}C (at ETNP) or ^{14}C (ETSP). Data were fitted to a photosynthesis–irradiance model to calculate maximum rates (GCP$_{max}$) and the initial slope of the curve (α), an index of the photosynthetic efficiency at low light (values in the main text). Error bars represent the SE.

Tracking O_2 consumption during our experiments allowed for estimates of aerobic respiration rates. O_2 consumption curves were linear down to about 50 nmol·L^{-1} during dark incubations (Fig. 2 A and D). Aerobic respiration by prokaryotes is generally driven by two classes of terminal oxidases: low-affinity terminal oxidases (LATO) with a half saturation constant (K_m) of about 200 nmol O_2·L^{-1} and high-affinity terminal oxidases (HATO) with K_m values of 3–8 nmol O_2·L^{-1} (18). Marine bacteria possessing HATO can decrease apparent K_m values of aerobic respiration down to less than 10 nmol O_2·L^{-1} (19), and a linear O_2 decrease may thus be expected down to about 50 nmol O_2·L^{-1}. Therefore, O_2 consumption rates (referred to as respiration for simplicity) obtained at concentrations >50 nmol·L^{-1} represent potential respiration rates (R^*) because they were measured above the threshold of O_2 limitation. The estimated R^* rates were significantly higher in the ETSP compared with the ETNP (Fig. 2 and Table S2), consistent with a higher microbial and particle abundance measured in the ETSP (Fig. 1 and Tables S1 and S2).

Experiments under the unique, almost anoxic conditions, of AMZs have not been performed in previous measurements of photosynthetic activity in the SCM (20). We conducted our experiments at O_2 levels below those sporadically detected by in situ measurements (up to 500 nmol·L^{-1}) but far above the K_m values for HATO. In this range, we can assume that gross community production of O_2 (GCP-O_2) can be calculated as the sum of NCP and R^*. We also validated these production calculations by simultaneously measuring the incorporation of inorganic carbon (using ^{13}C or ^{14}C) into biomass [gross community carbon production (GCP-C)], as has been done previously to quantify *Prochlorococcus* carbon fixation (20, 21). Both GCP-O_2 and GCP-C followed a classical photosynthesis–irradiance curve (Fig. 2 C and F), with maximum (GCP$_{max}$) values above saturating light intensities (E_k) of 10.5 ± 2.0 and 21.4 ± 9.3 μmol photons·m^{-2}·s^{-1} (0.5 and 1% of the incident light) for the ETNP and ETSP, respectively. The low E_k values reflect adaptation to the dim light environment, being similar to values found for the SCM community in the Arabian Sea (20) or in *Prochlorococcus* cultures (21). Above E_k, mean GCP$_{max}$-O_2 values in the ETNP and ETSP were 16.6 ± 9.1 and 52.5 ± 30.4 nmol O_2·L^{-1}·h^{-1}, respectively, and were generally consistent with maximum GCP-C rates (GCP$_{max}$-C: 8.1 ± 11.2 and 44.4 ± 30.3 nmol C·L^{-1}·h^{-1} in the ETNP and ETSP, respectively) (mean values of all stations ± SD in Table S3 and model in Fig. 2 C and F). The parameters describing the photosynthesis characteristics of the SCM community (maximum gross production rate, photosynthetic efficiency, and E_k) were similar to the values previously found for the SCM community of the Arabian Sea and the characterization of several *Prochlorococcus* isolates from the Pacific Ocean (20, 21). The values found for the ETNP were similar to those found

for the SCM of the Arabian Sea (20), whereas the ETSP SCM values were more similar to those from the laboratory cultures.

Although it is not yet possible to directly quantify in situ O_2 transformations in the AMZ, in situ GCP rates can be estimated based on water column chlorophyll concentrations and light conditions (Fig. S1). The light intensity at the SCM was variable and almost always substantially below 10 μmol photons·m^{-2}·s^{-1}. Under such conditions, O_2 production rates are lower than potential respiration rates (R^*), and the O_2 produced is immediately consumed by the microbial community, resulting in a cryptic O_2 cycle in the seemingly anoxic environment of the SCM (Fig. 1). However, at some stations the irradiance in the SCM was similar or close to the E_k. The occasional detection of low O_2 concentrations in the SCM (4, 8) (Table S2) may thus be explained by photosynthetic activity in the SCM increasing O_2 concentrations to measurable levels. Such daily changes are difficult to measure by discrete sampling, but recurrent measurements in the same water mass might reveal hourly and daily changes in the SCM.

Oxygen Production Coupling with Aerobic Microbial Processes. Even if undetectable, O_2 production in the SCM may support important (micro)aerobic metabolisms. To explore this prediction, we looked for signatures of such aerobic metabolism in available metatranscriptomes along the AMZ depth gradient in the ETNP during two cruises in 2014 and 2013, focusing on station T6 where the SCM was well developed and for which the metatranscriptome dataset was most comprehensive. Transcripts encoding terminal oxidases, including both LATO and HATO (Table S4), were detected at all depths (Fig. 3 and Fig. S2), including deep within the AMZ, where the transcript pool was dominated by sequences affiliated with diverse Gammaproteobacteria and Alphaproteobacteria (Fig. S3). The presence of oxidase transcripts within anoxic marine waters has been reported previously (13) and may reflect constitutive expression by groups at high abundance in the AMZ core, potentially to capitalize quickly on O_2 if it becomes available (22). The relative abundance of both LATO and HATO transcripts exhibits a local peak within the SCM compared with depths immediately above (base of oxycline) and below the SCM (Fig. 3 and Fig. S2). Similar trends were observed at stations T4 and T10, although limited sampling affected our ability to fully resolve oxidase distributions immediately above the SCM at these sites (Fig. S2). Together, these data provide evidence of a local peak in O_2 scavenging within the SCM.

Oxygen produced in the SCM may also be consumed through key steps of the OMZ nitrogen cycle. Comparatively high rates of autotrophic nitrification (ammonia and nitrite oxidation) are known to occur close to the oxic–anoxic boundary of AMZs (10). Here transcripts affiliated with ammonia oxidizing bacteria
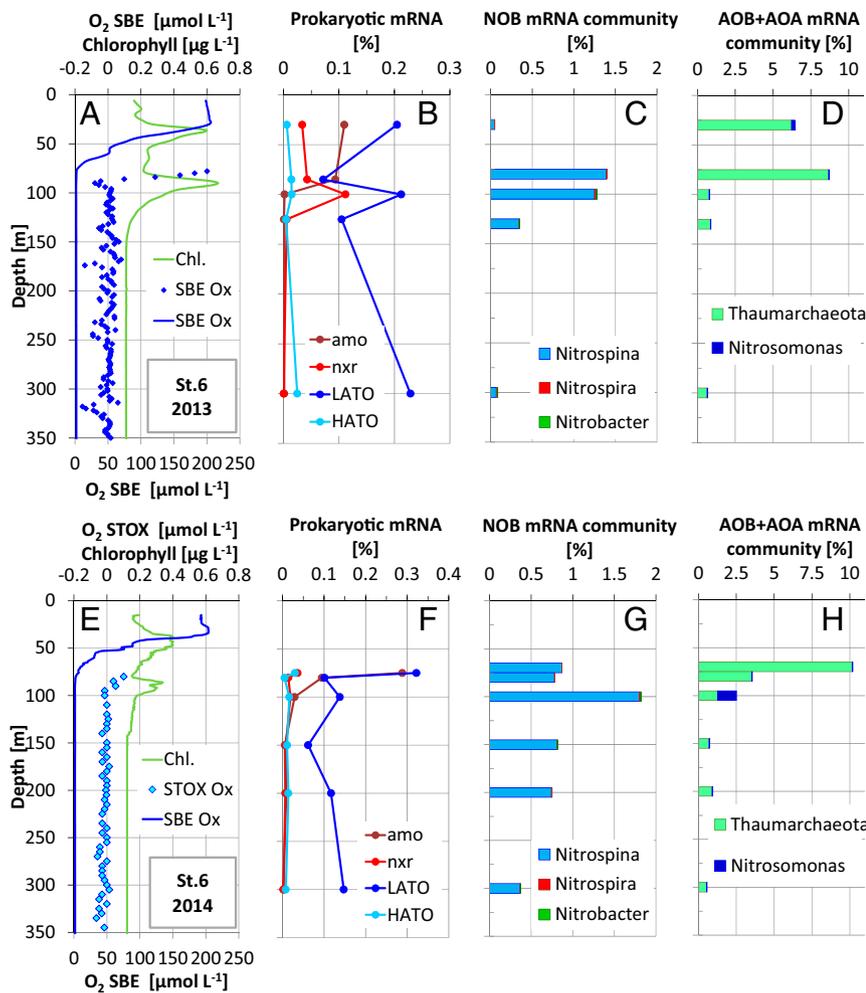
Fig. 3. Water column dissolved oxygen (O_2), chlorophyll concentrations (Chl.), and microbial transcript abundances at station T6 in the ETNP in (*A–D*) 2013 and (*E–H*) 2014. (*A* and *E*) O_2 based on SBE and STOX sensor measurement and chlorophyll inferred from in vivo fluorescence. (*B* and *F*) Abundances of transcripts encoding LATO and HATO, *amo*, and *nxr*, as a percentage of total prokaryotic mRNA. (*C* and *G*) Taxonomic classification of total mRNA affiliated with NOB and (*D* and *H*) AOB (Nitrosomonas) and AOA (Thaumarchaeota), as a percentage of total prokaryotic mRNA.

(AOB) and ammonia oxidizing archaea (AOA), notably those encoding the ammonia monooxygynase (*amo*) enzyme catalyzing aerobic ammonia oxidation, peaked in the upper part of the oxycline and declined in abundance into the core of the ETNP AMZ (Fig. 3 and Fig. S2). In contrast, transcripts of nitrite oxidizing bacteria (NOB), primarily those of the marine NOB genus *Nitrospina*, spiked within the SCM, coinciding in most cases with a local enrichment in transcripts encoding nitrite oxidoreductase (*nxr*) (Fig. 3 and Fig. S2). A prior study showed that potential nitrite oxidation rates at station T6 in the ETNP peaked in the anoxic SCM at 10.8 nmol $N \cdot L^{-1} \cdot h^{-1}$, a rate approximately double that of the maximal O_2 respiration rate measured in this study (Table S3). Taking the stoichiometry of nitrite oxidation into account, we can infer that most of the measured O_2 consumption (R^*) could be due to nitrite oxidation. The nitrite oxidation rates reported at the same stations were measured at low O_2 concentrations (<80 $nmol \cdot L^{-1}$), and we assume that the conditions were similar to our incubations, suggesting that the previous nitrite oxidation and our present R^* rates are directly comparable. The balance between heterotrophic and nitrite oxidizer O_2 consumption may, however, vary as a function of the actual O_2 concentration in the 0 to ~100 $nmol \cdot L^{-1}$ range that we measured in the ETNP SCM (Table S2). The cooccurrence of elevated *Nitrospina* transcription and nitrite oxidation rates in the SCM suggests that NOB is fueled by local O_2 production.

Implications for Oxygen Minimum Zones. The results of this study indicate that the SCM is a significant source of O_2 for both nitrite and organic matter oxidation, as well as a source of fixed carbon. Total productivity in terms of O_2 released and C fixed in

the SCM was calculated by integrating the GCP profiles (Fig. S1) over a diel cycle, using measured (ETSP) or estimated (ETNP) scalar irradiance profiles (Fig. S4 and Table 1). Higher chlorophyll and estimated irradiance values at the SCM in the ETNP off Mexico resulted in higher mean production rates (0.83/0.39 mmol $O_2/C \cdot m^{-2} \cdot d^{-1}$) compared with the ETSP off Peru (0.32/0.31 mmol $O_2/C \cdot m^{-2} \cdot d^{-1}$). Although in situ light attenuation profiles were used for the ETNP, cloud coverage and other local factors reducing the incident light could not be included in the calculations,

Table 1. Depth-integrated oxygen production and carbon fixation rates

Station	GCP, mmol·m⁻²·d⁻¹	
	O_2	C
ETNP–Mexico		
T4	0.43	0.15
F4	1.70	0.19
T7	0.48	0.13
T9	0.97	0.93
T10	0.59	0.55
	0.83 ± 0.53	0.39 ± 0.35
ETSP–Peru		
am_04	0.03	0.02
am_25	0.03	0.03
am_28	0.91	0.87
	0.32 ± 0.51	0.31 ± 0.49

and therefore, the production values should be taken as maximum values. Productivity was also highly variable among sites (0.43–1.70/0.15–0.95, and 0.03–0.91/0.02–0.87 mmol $O_2/C \cdot m^{-2} \cdot d^{-1}$ for ETNP and ETSP, respectively), reflecting the heterogeneous spatial distribution of the SCM (Fig. 1 and Tables S1 and S2).

Although primary production in surface waters largely exceeds these values (23), the vast majority of surface production is remineralized before reaching the AMZ core. Indeed, the range of particulate organic carbon supply to the AMZ is 0.83–7.81 mmol $C \cdot m^{-2} \cdot d^{-1}$ (11, 24) in the ETNP or 1.52–14.70 mmol $C \cdot m^{-2} \cdot d^{-1}$ in the ETSP (25). This wide range highlights the variability in export rates in these regions. Nonetheless, comparing these estimations with our data, the carbon production in the SCM could provide 5–47% and 2–20% of the organic matter supplied to the anoxic waters of the ETNP and ETSP, respectively, where part of it is then mineralized by dissimilatory nitrate reduction to nitrite and denitrification (8, 11, 23, 26). Nitrate respiration to nitrite appears as the dominant mineralization step in the ETNP (8), and mineralization rates of about 1 mmol $C \cdot m^{-2} \cdot d^{-1}$ can be calculated from published data (7, 23). These rates are close to the C fixation rate in the SCM, highlighting the relevance of the SCM in OMZ metabolism.

Global warming is expected to result in shoaling of the OMZ oxycline and overall expansion of OMZ volumes (27). Mesoscale physical processes such as local upwelling and anticyclonic eddies that shoal the oxic–anoxic boundary have been shown to enhance the development of SCMs (15, 16). Oxycline shoaling increases the light intensities in the anoxic cores of the AMZs, thereby potentially stimulating the photosynthetic community. The effects of these changes on microbial communities and microbial biogeochemical cycling in AMZs are difficult to predict, although significant changes in carbon, nitrogen, and sulfur cycling are expected (27). Our data show a significant carbon supply to the anoxic core of the Pacific AMZs by SCM photosynthetic activity, and it is likely that the situation is similar in the Arabian Sea. Although we did not measure nitrogen transformation processes, the nitrifying community was also enriched at the SCM, potentially reflecting elevated metabolic rates. A shoaling of the AMZ coupled with increases in irradiance and SCM photosynthetic activity would increase the carbon and daytime oxygen supply to the upper part of the AMZ. Shoaling of the AMZ due to global warming could thus lead to more extensive areas with high rates of SCM biological activity, with the diel oxic/anoxic cycles of these SCMs influencing marine productivity and coupled global nitrogen cycling.

Materials and Methods

Sampling Sites and in Situ Measurements. The two main oxygen minimum zones of the ETSP and ETNP were investigated during two cruises during 2014: the Activities of Research Dedicated to the Minimum of Oxygen in the Eastern Pacific (AMOP) cruise on the R/V *L'Atalante* to the ETSP off Peru during late January and February 2014 and the Oxygen Minimum Zone Microbial Biogeochemistry Expedition 2 (OMZoMBiE2) cruise on the R/V *New Horizon* to the ETNP region off Mexico during May–June 2014. Profiles of physical and chemical variables were obtained with a Seabird SBE-911 CTD system, equipped with a SBE 43 oxygen sensor and a Seapoint Chlorophyll Fluorimeter (R/V *New Horizon*) or a Chelsea Aqua 3 fluorimeter (R/V *L'Atalante*). CTD sensors were calibrated according to the manufacturer. The fluorometers used for the determination of chlorophyll were calibrated using pure chlorophyll solutions in 90% acetone (from 0.1 to 100 μg/L). In the ETNP, a pump profiling system (PPS) was also used for water collection. High-resolution O_2 profiling was performed during the CTD and PPS casts during the ETNP cruise. A high-resolution STOX sensor (2, 28) was used to measure O_2 concentration at nanomolar levels as described previously (2, 4).

Flow Cytometry Analysis. Samples for cell counts were taken at several depths from the rosette (ETNP and ETSP) and the PPS (ETNP), fixed with glutaraldehyde and stored at −80 °C until analysis. Cell abundance was determined by flow cytometry using a FACSCalibur flow cytometer (Beckton Dickinson). *Prochlorococcus*, *Synechococcus*, and other autofluorescent cells (identified as picoeukaryotes) were counted in untreated samples, whereas autofluorescent plus nonautofluorescent cells (bacteria + archaea, referred as total microbial community) were analyzed by staining the cells with SYBR Green (Molecular Probes) as described previously (29, 30).

Oxygen Production and Carbon Fixation Measurements. Water samples from the SCM (summarized in Table S1) were collected using Niskin bottles or a PPS. To minimize the O_2 leaking from the polymers of the Niskin bottles, the water was transferred to a 20-L glass bottle previously purged with N_2 gas as soon as the rosette was on deck. If the samples were collected using the PPS, the 20-L glass bottle purged with N_2 gas was filled directly from the outlet of the PPS. A certain O_2 contamination (1–5 μmol·L^{-1}) during the sampling procedure could not be avoided, and the seawater was therefore immediately degassed in the 20-L bottle by bubbling with N_2 + 0.05% CO_2. A STOX sensor was inserted inside the bottle to determine when anoxia was approached (<100 nmol O_2·L^{-1}). After adjusting the O_2 concentration to 100–400 nmol·L^{-1}, samples were siphoned to custom made incubation vessels (n = 12–16) (Fig. S5) (31, 32), containing either STOX sensors (ETSP) or a combination of STOX and optode sensors with a measuring range of 0–1,000 nmol·L^{-1} (32, 33) (ETNP). Each vessel was placed inside a light incubation tube immersed in a constant temperature water bath, enabling maintenance of in situ temperature (14–15 °C) and quantification of very low O_2 transformation rates. The light incubation tubes consisted of a black PVC tube with white LEDs (LF06S-W3F-850; OSRAM) installed along the whole periphery of the tube and with a custom-built waterproof magnetic stirrer fitted at the bottom. The LEDs were covered with a blue filter (131 Marine Blue filter; LEE Filters) to simulate the in situ light spectrum. Oxygen concentrations (Fig. 2) throughout the incubation period (8–12 h) were measured in treatments spanning a range of bluish light intensities slightly above maximum in situ levels (10, 20, and 40 μmol photons·m^{-2}·s^{-1}) and in darkness (n = 3–4, per treatment). Rates of oxygen consumption or production (here named NCP) were obtained by linear regression of the oxygen evolution during the incubations. GCP rates were calculated by subtracting the mean respiration value (NCP rate measured in darkness) from the NCP rates measured at different irradiances.

Rates of carbon incorporation were measured simultaneously during the incubations for oxygen measurements using stable (ETNP) or radioactive (ETSP) isotopes. Incubations amended with Na^{14}C-HCO$_3$ (450 μCi/L final concentration) were done in parallel incubation bottles of only 110 mL (but otherwise similar to the one described in Fig. S5) following the procedure described by Telling et al. (34). Incubations amended with Na^{13}C-HCO$_3$ (0.27 mM ^{13}C final concentration) were done in the same incubation bottles used for O_2 measurements. Incorporation of ^{14}C was measured by counting on a Perking Elmer Tri-Carb 2900 TR scintillation counter, whereas the ^{13}C incorporation was analyzed in an Elemental Analyzer (Thermo Elemental Analyzer Flash EA 1112 HT) coupled to an Isotope Ratio Mass Spectrometer (Delta V; Thermo Scientific). The ^{13}C enrichment in the produced organic carbon was calculated as the difference between the amounts of ^{13}C in the sample minus the natural ^{13}C abundance measured on blank filters. Decays per minute values (^{14}C incubations) and ^{13}C incorporation were converted to ^{12}C uptake values or GCP (nmol C·L^{-1}·h^{-1}) rates using the formula described in Telling et al. (34).

Rates Modeling and Upscaling of Processes. The photosynthesis–irradiance model described by Jassby and Platt (35) was fitted to the measured GCP (nmol·L^{-1}·h^{-1}) rates for both O_2 production and C assimilation (Fig. 2), being

$$GCP = GCP_{max} \times \tanh(\alpha \times E/GCP_{max}),$$

where GCP_{max} (nmol·L^{-1}·h^{-1}) is the maximum gross community production rate, reached at saturating irradiances, tanh is the hyperbolic tangent, α [(nmol·L^{-1}·h^{-1})(μmol photons·m^{-2}·s^{-1})$^{-1}$] is an index of the photosynthetic efficiency, and E (μmol photons·m^{-2}·s^{-1}) is the spherical irradiance.

The obtained parameters were normalized by the chlorophyll concentration and used to estimate the in situ O_2 production and C fixation using the light and chlorophyll profiles measured in the SCM by the fluorescence and photosynthetic active radiation (PAR) sensors connected to the CTD (ETSP cruise) or the PPS (ETNP cruise). During the ETSP cruise off Peru, casts were consistently repeated every 3–4 h, and thus, the light profiles from the CTD were used in our calculations. During the ETNP cruise, light profiles measured with the PPS during daytime were normalized to the incident irradiance at the surface. The light attenuation profiles were assumed to be constant at each station, and the incident irradiance was used to calculate the change in light profile during the day. The values of incident irradiance were taken from the closest National Radiation station located in San Diego (National Solar Radiation Database, National Oceanic and Atmospheric Administration, United States).

Metatranscriptome Analysis. Community cDNA sequencing was used to characterize microbial gene transcription in biomass (retained on 0.22-μm filters) from a subset of AMZ samples at the ETNP region off Mexico (Tables S4 and S5). These included samples collected during the OMZoMBiE2 cruise (2014) and a subset of samples previously reported by Padilla et al. (36). Seawater from discrete depths spanning the oxic zone, SCM, lower oxycline, upper AMZ, and AMZ core was collected using Niskin bottles or the PPS. The sampling, preservation, RNA extraction, and sequencing were done following the procedure described by Padilla et al. (36). Barcoded sequences were demultiplexed, and low-quality reads (Phred score < 25) were removed. Paired-end sequences were merged using custom scripts incorporating the FASTX toolkit (hannonlab.cshl.edu/fastx_toolkit/index.html) and USEARCH algorithm, with criteria of minimum 10% overlap and 95% nucleotide identity within the overlapping region. Ribosomal RNA (rRNA) transcripts were identified by riboPicker (37) and removed from the analysis. Merged nonrRNA sequences were queried via DIAMOND using sensitive search parameters (38) against the National Center for Biotechnology Information (NCBI)-nr database (November 2013). DIAMOND-identified protein-coding transcripts were assigned a functional annotation based Kyoto Encyclopedia of Genes and Genomes (KEGG) orthology (KO) identifiers (39) using Metagenome Analyzer 5 (MEGAN5) (40), with taxonomic classification assigned using the lowest common ancestor (LCA) algorithm in MEGAN5 based on the NCBI taxonomy. Counts per KO were normalized to the total number of protein coding transcripts classified within bacteria and archaea (i.e., prokaryotes). Transcripts encoding LATO and HATO, *nxr*, and *amo* (all subunits) were identified by the KO identifiers listed in Table S4.

NOB abundances were determined by taxonomic LCA assignment according to NCBI taxonomy of DIAMOND-identified mRNA transcripts normalized to the total number of prokaryotic mRNA sequences. Taxonomic affiliation of both LATO and HATO were also assigned according to NCBI taxonomy via the LCA algorithm in MEGAN5.

1. Paulmier A, Ruiz-Pino D (2009) Oxygen minimum zones (OMZs) in the modern ocean. *Prog Oceanogr* 80:113–128.
2. Revsbech NP, Thamdrup B, Dalsgaard T, Canfield DE (2011) Construction of STOX oxygen sensors and their application for determination of O₂ concentrations in oxygen minimum zones. *Research on Nitrification and Related Processes*, Methods in Enzymology, ed Klotz MG (Elsevier, San Diego), Part A, Vol 486, pp 325–341.
3. Thamdrup B, Dalsgaard T, Revsbech NP (2012) Widespread functional anoxia in the oxygen minimum zone of the Eastern South Pacific. *Deep Sea Res Part I Oceanogr Res Pap* 65:36–45.
4. Tiano L, et al. (2014) Oxygen distribution and aerobic respiration in the north and south eastern tropical Pacific oxygen minimum zones. *Deep Sea Res Part I Oceanogr Res Pap* 94:173–183.
5. Ulloa O, Canfield DE, DeLong EF, Letelier RM, Stewart FJ (2012) Microbial oceanography of anoxic oxygen minimum zones. *Proc Natl Acad Sci USA* 109:15996–16003.
6. Bristow LA, et al. (2017) N2 production rates limited by nitrite availability in the Bay of Bengal oxygen minimum zone. *Nat Geosci* 10:24–29.
7. Canfield DE, et al. (2010) A cryptic sulfur cycle in oxygen-minimum-zone waters off the Chilean coast. *Science* 330:1375–1378.
8. Ganesh S, et al. (2015) Size-fraction partitioning of community gene transcription and nitrogen metabolism in a marine oxygen minimum zone. *ISME J* 9:2682–2696.
9. Codispoti L, et al. (2001) The oceanic fixed nitrogen and nitrous oxide budgets: Moving targets as we enter the anthropocene? *Sci Mar* 65:85–105.
10. Dalsgaard T, Thamdrup B, Farias L, Revsbech NP (2012) Anammox and denitrification in the oxygen minimum zone of the eastern South Pacific. *Limnol Oceanogr* 57: 1331–1346.
11. Babbin AR, Keil RG, Devol AH, Ward BB (2014) Organic matter stoichiometry, flux, and oxygen control nitrogen loss in the ocean. *Science* 344:406–408.
12. Stewart FJ, Ulloa O, DeLong EF (2012) Microbial metatranscriptomics in a permanent marine oxygen minimum zone. *Environ Microbiol* 14:23–40.
13. Kalvelage T, et al. (2015) Aerobic microbial respiration in oceanic oxygen minimum zones. *PLoS One* 10:e0133526.
14. Lavin P, González B, Santibáñez JF, Scanlan DJ, Ulloa O (2010) Novel lineages of Prochlorococcus thrive within the oxygen minimum zone of the eastern tropical South Pacific. *Environ Microbiol Rep* 2:728–738.
15. Goericke R, Olson RJ, Shalapyonok A (2000) A novel niche for Prochlorococcus sp in low-light suboxic environments in the Arabian Sea and the Eastern Tropical North Pacific. *Deep Sea Res Part I Oceanogr Res Pap* 47:1183–1205.
16. Cepeda-Morales J, Beier E, Gaxiola-Castro G, Lavín M, Godínez V (2009) Effect of the oxygen minimum zone on the second chlorophyll maximum in the Eastern Tropical Pacific off Mexico. *Cienc Mar* 35:389–403.
17. Bristow LA, et al. (2016) Ammonium and nitrite oxidation at nanomolar oxygen concentrations in oxygen minimum zone waters. *Proc Natl Acad Sci USA* 113: 10601–10606.
18. Morris RL, Schmidt TM (2013) Shallow breathing: Bacterial life at low O(2). *Nat Rev Microbiol* 11:205–212.
19. Gong X, Garcia-Robledo E, Schramm A, Revsbech NP (2015) Respiratory kinetics of marine bacteria exposed to decreasing oxygen concentrations. *Appl Environ Microbiol* 82:1412–1422.
20. Johnson Z, et al. (1999) Energetics and growth kinetics of a deep Prochlorococcus spp. population in the Arabian Sea. *Deep Sea Res Part II Top Stud Oceanogr* 46:1719–1743.
21. Moore LR, Chisholm SW (1999) Photophysiology of the marine cyanobacterium Prochlorococcus: Ecotypic differences among cultured isolates. *Limnol Oceanogr* 44: 628–638.
22. Tsementzi D, et al. (2016) SAR11 bacteria linked to ocean anoxia and nitrogen loss. *Nature* 536:179–183.
23. Kalvelage T, et al. (2013) Nitrogen cycling driven by organic matter export in the South Pacific oxygen minimum zone. *Nat Geosci* 6:228–234.
24. Devol AH, Hartnett HE (2001) Role of the oxygen-deficient zone in transfer of organic carbon to the deep ocean. *Limnol Oceanogr* 46:1684–1690.
25. Escribano R, et al. (2004) Biological and chemical consequences of the 1997–1998 El Niño in the Chilean coastal upwelling system: A synthesis. *Deep Sea Res Part II Top Stud Oceanogr* 51:2389–2411.
26. Ward BB (2013) Oceans. How nitrogen is lost. *Science* 341:352–353.
27. Gilly WF, Beman JM, Litvin SY, Robison BH (2013) Oceanographic and biological effects of shoaling of the oxygen minimum zone. *Annu Rev Mar Sci* 5:393–420.
28. Revsbech NP, et al. (2009) Determination of ultra-low oxygen concentrations in oxygen minimum zones by the STOX sensor. *Limnol Oceanogr Methods* 7:371–381.
29. Lebaron P, Parthuisot N, Catala P (1998) Comparison of blue nucleic acid dyes for flow cytometric enumeration of bacteria in aquatic systems. *Appl Environ Microbiol* 64: 1725–1730.
30. Grégori G, Denis M, Seorbati S, Citterio S (2001) Resolution of viable and membrane-compromised free bacteria in aquatic environments by flow cytometry. Curr Protoc Cytom 11:11.15.1–11.15.7.
31. Tiano L, Garcia-Robledo E, Revsbech NP (2014) A new highly sensitive method to assess respiration rates and kinetics of natural planktonic communities by use of the switchable trace oxygen sensor and reduced oxygen concentrations. *PLoS One* 9: e105399.
32. Garcia-Robledo E, Borisov S, Klimant I, Revsbech NP (2016) Determination of respiration rates in water with sub-micromolar oxygen concentrations. *Front Marine Sci* 3:244.
33. Lehner P, et al. (2015) LUMOS—A sensitive and reliable optode system for measuring dissolved oxygen in the nanomolar range. *PLoS One* 10:e0128125.
34. Telling J, et al. (2010) Measuring rates of gross photosynthesis and net community production in cryoconite holes: A comparison of field methods. *Ann Glaciol* 51: 153–162.
35. Jassby A, Platt T (1976) Mathematical formulation of the relationship between photosynthesis and light for phytoplankton. *Limnol Oceanogr* 21:540–547.
36. Padilla CC, et al. (2016) NC10 bacteria in marine oxygen minimum zones. *ISME J* 10: 2067–2071.
37. Schmieder R, Lim YW, Edwards R (2012) Identification and removal of ribosomal RNA sequences from metatranscriptomes. *Bioinformatics* 28:433–435.
38. Buchfink B, Xie C, Huson DH (2015) Fast and sensitive protein alignment using DIAMOND. *Nat Methods* 12:59–60.
39. Kanehisa M, Goto S (2000) KEGG: Kyoto encyclopedia of genes and genomes. *Nucleic Acids Res* 28:27–30.
40. Huson DH, Mitra S, Ruscheweyh H-J, Weber N, Schuster SC (2011) Integrative analysis of environmental sequences using MEGAN4. *Genome Res* 21:1552–1560.

Supporting Information

Garcia-Robledo et al. 10.1073/pnas.1619844114
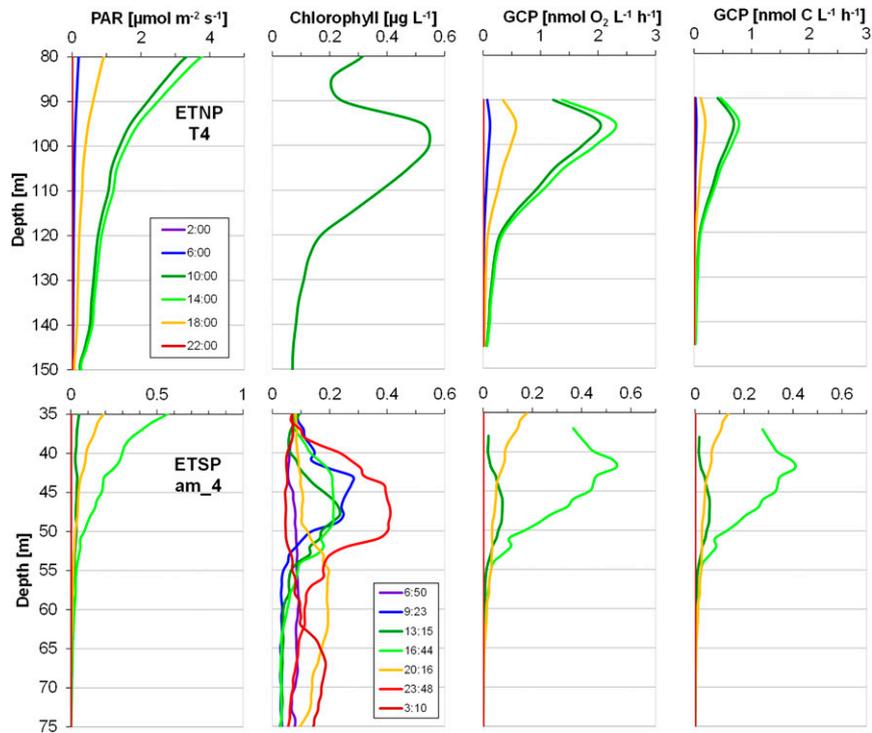
Fig. S1. PAR, chlorophyll, and in situ gross oxygen production and carbon fixation rates in the SCM estimated from onboard experimental data for O_2 metabolism and C fixation. GCP rates were calculated only at the SCM, considered as the water layer extending from the minimum fluorescence value between the peaks to the bottom of the photic layer. An oceanic station with a deeper SCM (T4) off Mexico (ETNP, *Upper*) and a coastal station with a shallow SCM (am_4) off Peru (ETSP, *Lower*). Note the different scales.
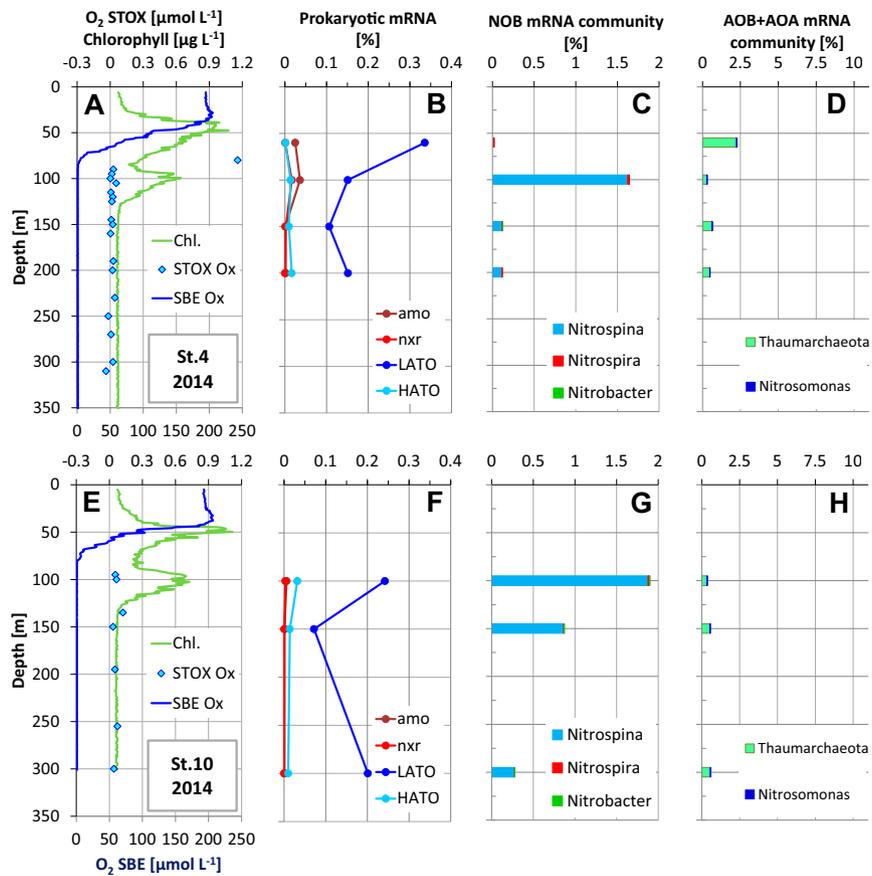
Fig. S2. Water column dissolved oxygen (O$_2$) and chlorophyll concentrations and microbial transcript abundances at stations (*A–D*) T4 and (*E–H*) T10 in the ETNP in 2014. (*A* and *E*) O$_2$, based on SBE and STOX senor measurement, and chlorophyll inferred from in vivo fluorescence. (*B* and *F*) Abundances of transcripts encoding LATO and HATO, *amo*, and *nxr*, as a percentage of total prokaryotic mRNA. (*C* and *G*) Taxonomic classification of total mRNA affiliated with NOB and (*D* and *H*) AOB and AOA, as a percentage of total prokaryotic mRNA.
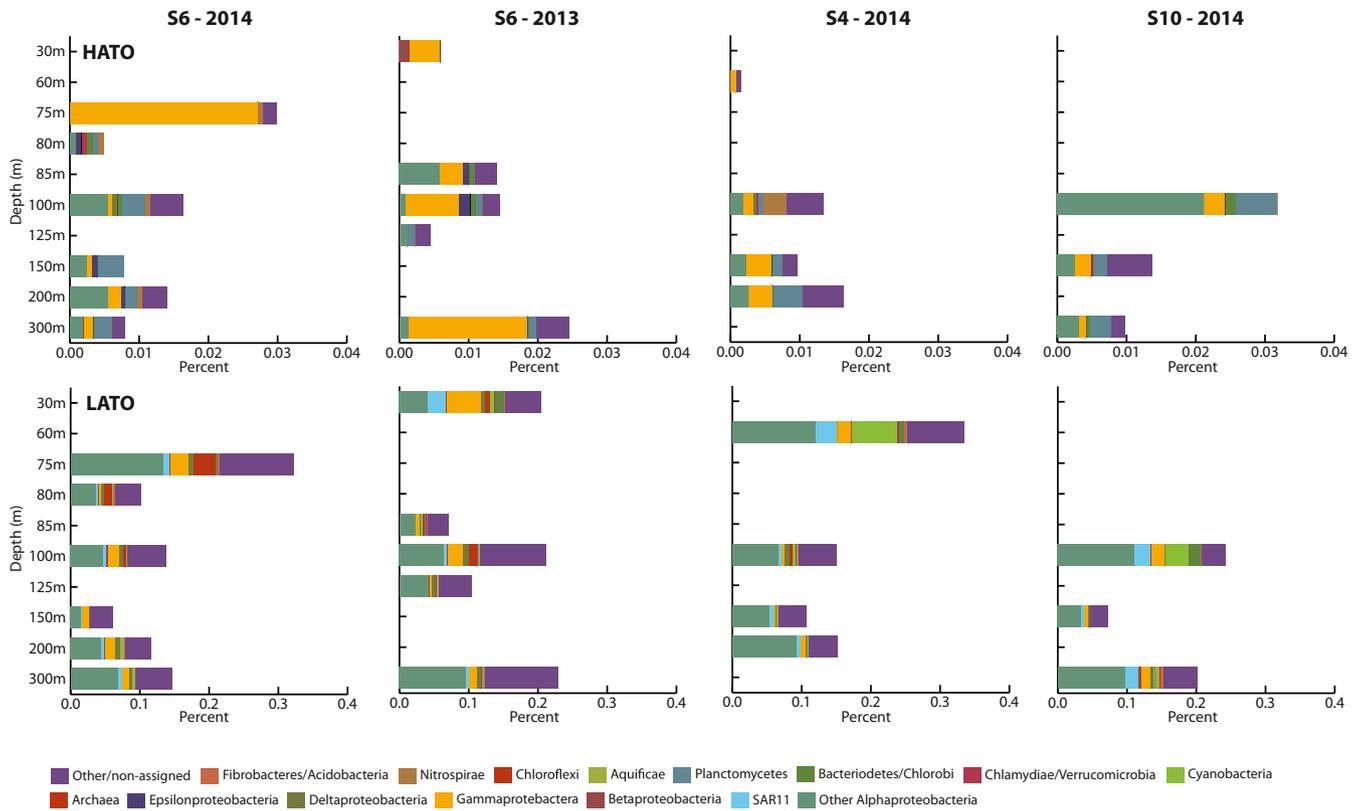
Fig. S3. Taxonomic identities of terminal oxidases. Taxonomic assignment of (*Upper*) HATO and (*Lower*) LATO at stations T4, T6, and T10 off Mexico in 2014 and T6 in 2013 as determined via lowest common ancestor binning in MEGAN5. Abundances are presented as the percentage of total prokaryotic mRNA from each sample.
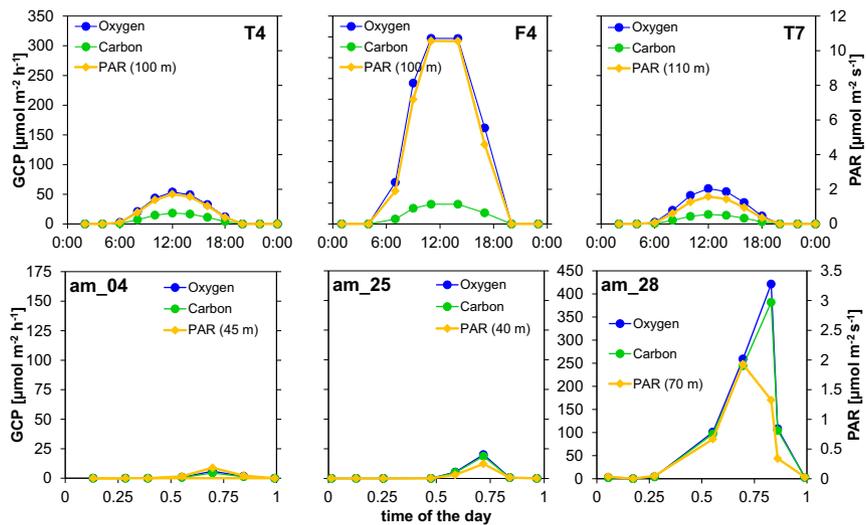
Fig. S4. Depth integration of in situ gross oxygen production and carbon fixation rates. Three stations off Mexico (T4, F4, T7; *Upper*) and off Peru (am_04, am_25, and am_28; *Lower*) were selected as examples. Modeled in situ gross oxygen production and carbon fixation rate profiles were integrated with depth to calculate the aerial contribution of the SCM. We used only GCP rates from the SCM, being delimited as the water layer extending from the minimum fluorescence value between the primary and secondary chlorophyll maxima to the bottom of the photic layer. Light at the depth where the maximum fluorescence value was measured is also shown as reference.
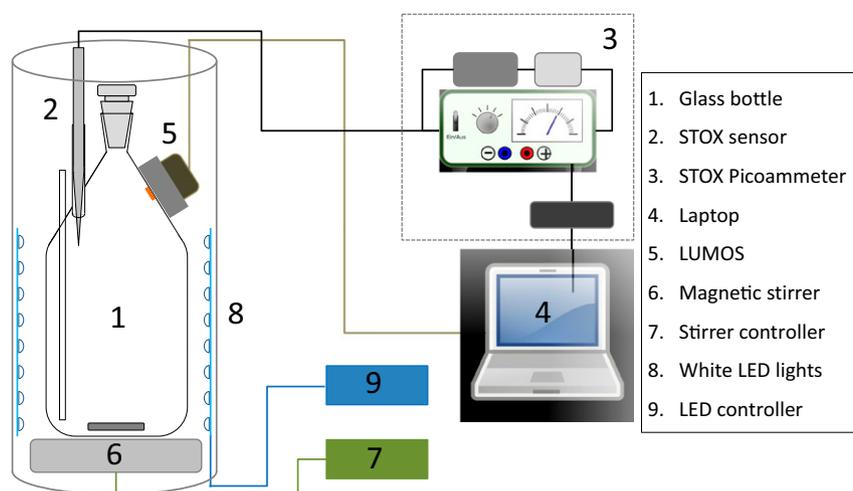
Fig. S5. Experimental setup for measurement of O$_2$ production/consumption. Glass bottle (labeled as 1) with a volume of 1160 mL. A series of modifications were done to a standard Schott–Duran glass bottle including (*i*) the insertion of a long open glass tube (internal diameter 2.5 mm) for pressure compensation and for the injection of calibration solution or tracers; (*ii*) the addition of a short 8.1-mm (inner diameter) glass tube for insertion of the STOX sensor (labeled as 2) or a solid 8-mm glass bar if STOX sensors were not used; (*iii*) a modification of the bottle neck to accommodate a ground glass stopper (internal diameter 12 mm) so that the inner part of the bottle could be accessed; and (*iv*) insertion of a sensing dot for optode-based measurements that was glued onto the inner surface of the bottle, whereas the reading device (LUMOS) was positioned on the outside, held by a PVC frame glued to the bottle. STOX sensors (labeled as 2) were connected to a picoammeter (labeled as 3) equipped with an external battery and a switch for the periodic polarization of the front guard of the sensor. The signal from the picoammeter was fed into an A/D converter connected to a laptop (labeled as 4). The LUMOS (labeled as 5) device was directly connected to the laptop. A magnetic stirrer (labeled as 6) and a controller (labeled as 7) ensured homogeneous mixing of the water in the bottle by a glass coated magnet. A white LED system surrounded the bottle (labeled as 8) to ensure a homogeneous light distribution. The light intensity was modulated by an external controller (labeled as 9), and the light spectrum of the SCM was simulated by coating the LEDs with a Marine Blue filter (LEE Filters). The LEDs were installed within a nontransparent PVC tube. The incubation bottles and associated lighting and stirring equipment were immersed into a water bath held at the in situ temperature (14 °C).

Table S1. Flow cytometry analysis of the SCM microbial community

Cruise	Station	Depth, m	Prochl., 10^4 cells per mL	Syn., 10^4 cells per mL	P.euk., 10^4 cells per mL	T.Microb., 10^5 cells per mL	Prochl., % photot.	Prochl., % total	Chl., µg·L^{-1}
OMZoMBiE2 (ETNP)	T4	100	5.06	0.29	0.001	3.56	94.5	12.4	0.55
	T7	80	2.99	0.66	0.000	3.95	81.8	6.9	0.15
	T9	90	6.97	0.74	0.009	4.76	90.3	12.6	0.67
	T10	110	5.99	0.45	0.002	8.67	93.0	6.4	0.52
	T3	115	1.76	0.08	0.001	2.12	95.4	7.6	0.20
	F12	85	5.56	0.43	0.000	6.49	92.8	7.8	0.43
Mean		97	4.72	0.44	0.002	4.92	91.3	9.0	0.42
SD		14	1.96	0.24	0.003	2.33	5.0	2.8	0.21
AMOP'14 (ETSP)	am_4	50	13.80	0.30	0.006	3.49	97.8	28.1	0.13
	am_25	30	21.97	3.70	0.035	19.02	85.5	10.2	0.16
	am_28	60	18.96	3.06	0.012	14.66	86.0	11.2	0.21
Mean		47	18.25	2.35	0.018	12.39	89.8	16.5	0.16
SD		15	4.13	1.81	0.015	8.01	7.0	10.1	0.04

The abundance of *Prochlorococcus sp.* (Prochl.), *Synechococcus sp.* (Syn.), photosynthetic pico-eukaryotes (P.euk.), and total microbial community (T.Microb.) are expressed as cells per mL. The percentage of *Prochlorococcus sp.* in the phototrophic microbial community (% photot.) and in the total microbial community (% total) were also calculated. Mean chlorophyll values (Chl.) from in situ CTD measurements were added for comparison.

Table S2. Descriptive data and CTD measurements from within the SCM at sampled stations in both the ETNP and ETSP

Cruise	Station	Date (2014)	Offshore (K_m)	Depth, m	Beam transmission, %	Chlorophyll, μg·L^{-1}	O$_2$, μmol·kg^{-1}	T, °C	Density (σ_θ), kg·m^{-3}
OMZoMBiE2 (ETNP)	T4	15/05	140	100	88.92	0.54	0.002	14.2	26.0
	F4	18/05	150	100	88.93	0.54	0.013	14.1	25.8
	T7	21/05	70	95	89.10	0.38	0.439	15.6	25.6
	T7	21/05	70	90	89.04	0.24	—	15.1	25.8
	T9	22/05	125	90	—	0.67	0.002	14.3	26.0
	T10	24/05	190	100	88.61	0.64	0.000	14.6	25.9
	T3	27/05	230	110	89.49	0.25	0.314	14.1	26.0
	T3	27/05	230	105	88.94	0.44	0.102	14.5	25.9
	F13	01/06	280	90	88.62	0.75	0.006	14.4	25.9
Mean				98	88.96	0.49	0.112	14.6	25.9
SD				7	0.28	0.18	0.170	0.5	0.1
AMOP'14 (ETSP)	am_4	31/01	97	46	80.73	0.21	0.16	14.7	26.3
	am_25	14/02	30	45	79.68	0.30	0.07	14.7	25.8
	am_25	15/02	30	53	79.82	0.30	0.22	14.6	26.2
	am_28	17/02	125	70	80.25	0.20	0.04	13.6	26.2
	am_28	19/02	125	70	80.95	0.12	68.56	13.6	26.2
Mean				57	80.29	0.23	0.123	14.3	26.2
SD				12	0.55	0.08	0.083	0.6	0.2

Table S3. Summary of metabolic rates calculated from oxygen and carbon incorporation data

Cruise	Station	Depth, m	R^*, nmol O$_2$·L^{-1}·h^{-1}	GCP$_{max}$, nmol·L^{-1}·h^{-1} O$_2$	GCP$_{max}$, nmol·L^{-1}·h^{-1} C	α, (nmol·L^{-1}·h^{-1}) (μmol photons·m^{-2}·s^{-1})$^{-1}$ O$_2$	α, (nmol·L^{-1}·h^{-1}) (μmol photons·m^{-2}·s^{-1})$^{-1}$ C
OMZoMBiE2 (ETNP)	T4	100	2.6	13.3	2.4	1.26	0.2
	F4	100	5.7	8.8	1.1	0.75	0.1
	T7	95	5.3	8.0	2.6	0.61	0.2
	T7	90	6.9	10.0	0.0	0.76	0.0
	T9	90	3.2	35.5	30.3	3.19	3.1
	T10	100	7.1	19.4	9.2	1.77	0.8
	T3	110	17.4	16.8	3.1	1.32	0.4
	T3	105	11.4	—	—	1.60	—
	F13	90	8.2	21.3	—	1.89	—
Mean		98	7.5	16.6	6.9	1.46	0.69
SD		7	4.5	9.1	10.7	0.80	1.09
AMOP'14 (ETSP)	am_4	46	32.6	32.5	28.5	2.4	1.9
	am_25	45	20.1	32.1	33.1	1.61	1.02
	am_25	53	22.8	105.0	98.3	3.49	3.25
	am_28	70	25.7	51.9	35.2	2.11	2.01
	am_28	70	63.2	41.0	27.1	4.08	2.28
Mean		57	32.9	52.5	44.4	2.74	2.09
SD		12	17.6	30.4	30.3	1.02	0.80

Table S4. KEGG orthology identifiers used to screen metatranscriptomic datasets for terminal oxidase and nitrification marker genes

Function	Protein	Abbreviation	KEGG orthology identifier (KO)
Terminal oxidase	Cytochrome C	*LATO*	K02277, K02276, K02274, K15408, K02275, K02258, K02259
Terminal oxidase	cbb3	*HATO*	K00404, K00405, K15862, K00407, K00406
Terminal oxidase	bd	*HATO*	K00425, K00246
Nitrification	Nitrite oxidoreducatase	*nxr*	K00370, K00371
Nitrification	Ammonia monooxygenase	*amo*	K10944, K10945, K10946

Table S5. ETNP sequencing statistics

Year	Stn	Depth, m	Total	Read length, bp	nonrRNA	DIAMOND	MEGAN bacteria	MEGAN archaea	MEGAN Prok	Accession
2013	6	30	1,521,531	203	1,053,980	108,873	62,934	5,476	68,410	PRJNA263621*
		85	1,364,985	201	294,080	175,178	115,127	4,935	120,062	PRJNA263621*
		100	1,024,593	214	218,551	158,677	115,316	1,922	117,238	PRJNA263621*
		125	1,494,459	204	377,156	256,113	174,678	4,559	179,237	PRJNA263621*
		300	712,020	212	159,091	110,937	78,842	2,389	81,231	PRJNA263621*
2014	4	60	2,302,732	197	417,033	232,758	126,802	6,986	133,788	PRJNA305951
		100	2,520,169	199	805,179	359,336	258,010	15,993	274,003	PRJNA305951
		150	1,291,622	208	310,389	183,424	128,402	6,995	135,397	PRJNA305951
		200	1,212,126	205	253,637	155,219	110,453	5,938	116,391	PRJNA305951
	6	75	4,786,146	164	957,802	298,788	187,702	63,517	251,219	PRJNA277357[†]
		80	1,407,348	183	591,754	165,806	80,047	41,583	121,630	PRJNA305951
		100	1,601,640	183	611,712	192,294	133,385	13,799	147,184	PRJNA305951
		150	1,452,296	202	359,133	169,271	113,485	14,564	128,049	PRJNA305951
		200	2,325,341	177	482,694	210,303	158,319	5,971	164,290	PRJNA305951
		300	18,781,558	185	7,710,908	1,645,992	1,540,161	51,789	1,591,950	PRJNA277357[†]
	10	100	2,149,661	192	439,535	106,713	62,268	3,823	66,091	PRJNA277357[†]
		150	4,523,472	166	1,276,310	495,416	416,236	14,970	431,206	PRJNA277357[†]
		300	1,335,682	194	439,535	226,427	187,523	6,458	193,981	PRJNA277357[†]

Stn, stations in the ETNP; Total, number of sequences post trimming, merging, and quality control; Read length, average read length (bp) of merged and quality controlled sequences; nonrRNA, number of nonrRNA reads; DIAMOND, number of sequences with DIAMOND matches (bit score >50) to protein-coding sequences in the NCBI-nr database; MEGAN bacteria, number of reads assigned to the bacteria node using the lowest common ancestor (LCA) algorithm in MEGAN5; MEGAN archaea, number of reads assigned to the archaea node using the LCA algorithm in MEGAN5; MEGAN Prok, the sum of bacteria and archaea-assigned reads by the LCA algorithm; and Accession, NCBI accession number or BioProject ID.

*Samples collected in 2013 published in Ganesh et al. (8).

[†]Samples collected in 2014 published in Padilla et al. (35).